

## Structural and electrical properties of La(Sr,Ca)MnO<sub>3</sub> ceramics for NTC thermistors

Eun-Hui Kim<sup>a,†</sup>, Sam-Haeng Lee<sup>b,c,†</sup>, Byeong-Jun Park<sup>b</sup>, Jeong-Eun Lim<sup>b</sup>, Myung-Gyu Lee<sup>b,c</sup>, Joo-Seok Park<sup>c</sup>,  
Byung-Cheul Kim<sup>d</sup> and Sung-Gap Lee<sup>a,b,\*</sup>

<sup>a</sup>Dept. of Ceramics Engineering, Gyeongsang National University, Jinju 52828, Korea

<sup>b</sup>Dept. of Materials Engineering and Convergence Technology, RIGET, Gyeongsang National University, Jinju 52828, Korea

<sup>c</sup>Business Support Division, Korea Institute of Ceramic Engineering and Technology, Jinju 52851, Korea

<sup>d</sup>Dept. of Convergence Electronic Engineering, Gyeongsang National University, Jinju 52828, Korea

La<sub>0.7</sub>(Sr<sub>0.3-x</sub>Ca<sub>x</sub>)MnO<sub>3</sub> (0.1 ≤ x ≤ 0.25) ceramics were prepared using solid-state sintering. XRD measurements showed that all specimens showed rhombohedral polycrystalline structures. As the amount of Ca increased from 0.1 mol to 0.25 mol, sintered densities decreased from 5.8888 g/cm<sup>3</sup> to 5.5829 g/cm<sup>3</sup>. All specimens exhibited excellent NTCR properties of approximately 0.445–0.421 %/°C. The TCR property, B<sub>25/65</sub> constant, and resistivity at room temperature of the LSMO specimen doped with 0.2 mol Ca were 0.439 %/°C, 469 K, and 3.94 × 10<sup>4</sup> Ω-cm, respectively.

**Keywords:** La(Sr,Ca)MnO<sub>3</sub>, Thermistors, Hopping conduction, Structural properties, Electrical properties

### Introduction

Perovskite R<sub>1-x</sub>A<sub>x</sub>MnO<sub>3</sub> (R-trivalent ions of La, Pr, Nd etc., A-divalent ion of Ca, Sr, Ba etc.) ceramics exhibit various optical, electrical, and magnetic properties, depending on their composition and fabrication. Many studies have been conducted regarding their application to devices such as spintronics, non-volatile memory, and solid oxide fuel cells [1, 2]. The phase transition temperature (Curie temperature), crystalline structure, and magnetic properties of La<sub>1-x</sub>Sr<sub>x</sub>MnO<sub>3</sub> (LSMO) ceramics vary with their composition ratio [3]. LSMO ceramics have an especially high Curie temperature and low electrical resistance, compared to other ferromagnetic manganite system materials. In addition, when 0.2 ≤ x ≤ 0.5, they exhibit colossal magnetoresistant (CMR) properties for semi-metallic materials, which are defined by a complete spin polarization of the charge carrier when below Curie temperature [4]. The electrical and magnetic properties of LSMO ceramics are determined by the valence of the Mn ions, a mixture of Mn<sup>3+</sup> and Mn<sup>4+</sup>, and occur with localized electron hopping between Mn<sup>3+</sup> and Mn<sup>4+</sup> ions in the Mn-O octahedral sites. Consequently, the transport mechanism relies heavily on the structural parameters of the unit cell, such as the distance between the Mn-O ions and the angle between

the Mn-O-Mn ions. Hopping conduction to these neighboring sites typically represents a negative temperature coefficient (NTC) of resistance [5]. Many studies have been conducted on NTC thermistor materials and devices due to their increased utilization in industrial and home electronic components, such as in circuit compensation, automobiles, and in temperature measurement and control. For this study, Ba<sub>0.7</sub>Sr<sub>0.3</sub>MnO<sub>3</sub> ceramics were selected, from among all La<sub>1-x</sub>Sr<sub>x</sub>MnO<sub>3</sub> manganites, due to their superior electrical and magnetic properties. They were selected in their basic composition, and the structural and electrical properties were measured according to the amount of Ca added. The applicability of NTC thermistor devices was investigated.

### Experiment

La<sub>2</sub>O<sub>3</sub> (Aldrich, 99.99%), SrCO<sub>3</sub> (Aldrich, 99.99%), CaCO<sub>3</sub> (Aldrich, 99.99%), and Mn<sub>2</sub>O<sub>3</sub> (Alfa Aesar, 99%) were used as raw materials to fabricate La<sub>0.7</sub>(Sr<sub>0.3-x</sub>Ca<sub>x</sub>)MnO<sub>3</sub> (0.1 ≤ x ≤ 0.25). After weighing each raw material according to the composition formula, ethyl alcohol was used as a dispersion medium and the composition was mixed and then pulverized with a ball mill for 24 h using zirconia balls. The mixed and pulverized powders were calcined at 850 °C for 2 h. PVA 3% was added as a binder to the calcined powder, and the powder was sintered at 1,300 °C for 3 h. X-ray diffraction analysis (XRD, D8, Bruker), Field-emission scanning electron microscopy (FE-SEM, XL30S, Philips) and X-ray photoelectron spectra (XPS, VG Scientific ESCALAB 250) were used to analyze the structural properties of

<sup>†</sup>Eun-Hui Kim and Sam-Haeng Lee are co-first authors and contributed equally to this work.

\*Corresponding author:  
Tel : +82-10-2686-4427  
Fax: +82-55-772-1689  
E-mail: lsgap@gnu.ac.kr

the specimen. To measure the electrical properties, Ag electrodes were formed on both sides of the specimen by the screen printing method. Electrical properties were measured using a LCR meter (PM-6036, Fluke) and electrometer (Keithley 6517A).

## Results and Discussion

Fig. 1 shows a particle size analysis of the LSMO powder doped with 0.2 mol Ca after ball mill treatment. The bimodal particle size distribution, with an average size of 0.1  $\mu\text{m}$  and 2  $\mu\text{m}$ , is shown. No dependence on the composition ratio of Ca was observed. The dominant particle size was about 0.15  $\mu\text{m}$ .

Fig. 2 shows the (a) X-ray diffraction pattern and (b) lattice constant of various Ca-doped LSMO specimens. Regardless of the amount of Ca added, all specimens had rhombohedral crystal structures. As Ca ions (=0.099 nm) with small ionic radii were substituted with Sr (=0.113 nm) ions or La ions (=0.115 nm), the lattice constants decreased from 0.547 nm to 0.544 nm as the amount of Ca addition increased from 0.1 mol to 0.25 mol.

Fig. 3 shows the microstructure of the Ca-doped LSMO specimens. For the Ca composition ratio of  $0.1 \leq x \leq 0.2$ , the fracture plane of the specimen showed a transgranular fracturing pattern. This is because pores with large thermal expansion coefficients were distributed within the specimen, resulting in tensile stress on the pores, and compressive stresses on the matrix. Cracks formed through the pores and at the interfaces between the pores and matrix [6, 7]. However, for the specimens with a Ca composition ratio of 0.25 mol, pore size was larger and intergranular fracturing patterns were observed due to excessive addition of Ca ions having a small ionic radius. The internal stress generated by the contraction of the unit cells distributed at the grain boundaries. Although not shown in this paper, sintered

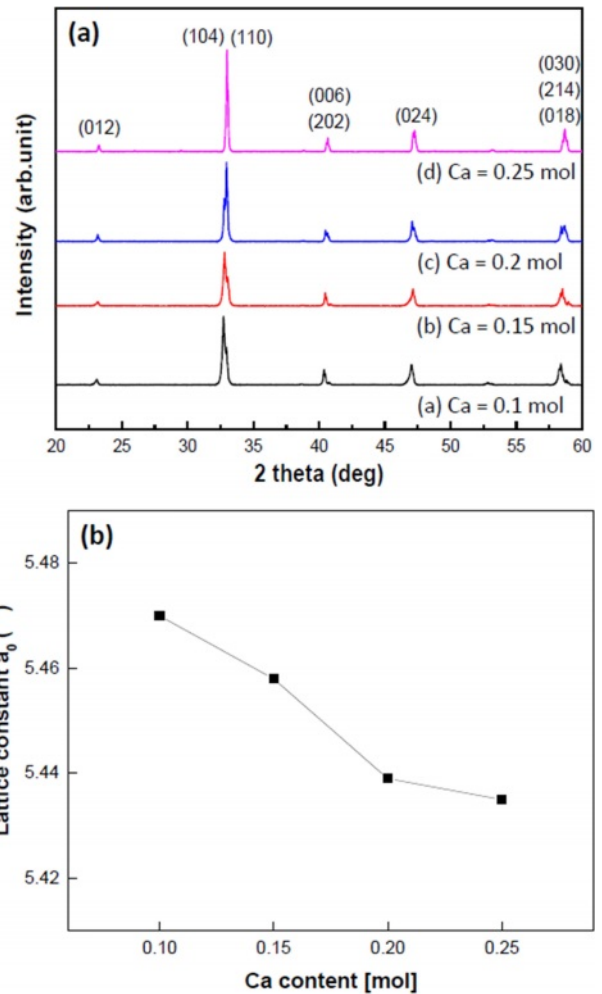


Fig. 2. (a) X-ray diffraction patterns and (b) Lattice constant of Ca-doped LSMO specimens.

densities decreased from 5.8888  $\text{g}/\text{cm}^3$  to 5.5829  $\text{g}/\text{cm}^3$  as the Ca composition ratio increased from 0.1 mol to 0.25 mol.

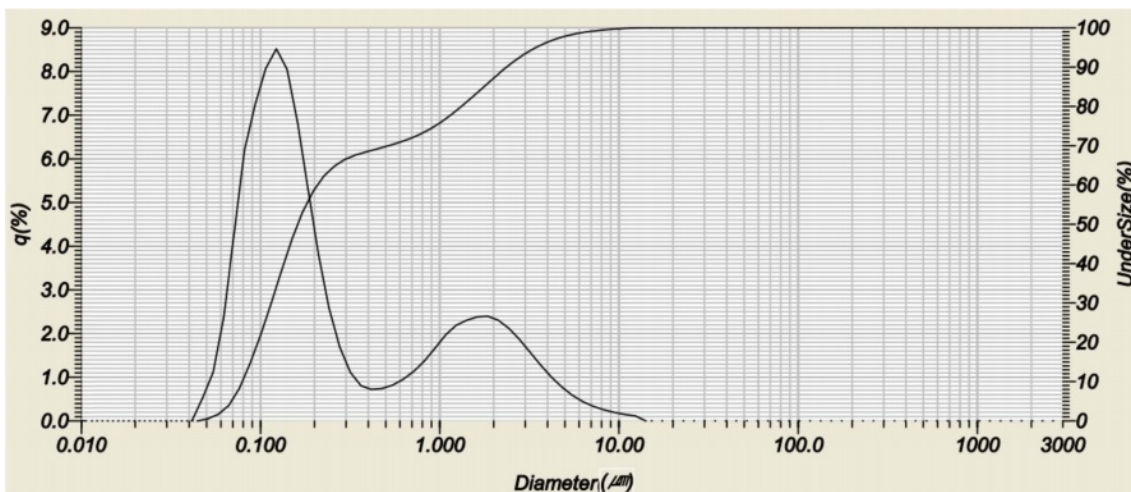


Fig. 1. Particle size analysis of LSMO powders doped with 0.2 mol Ca.

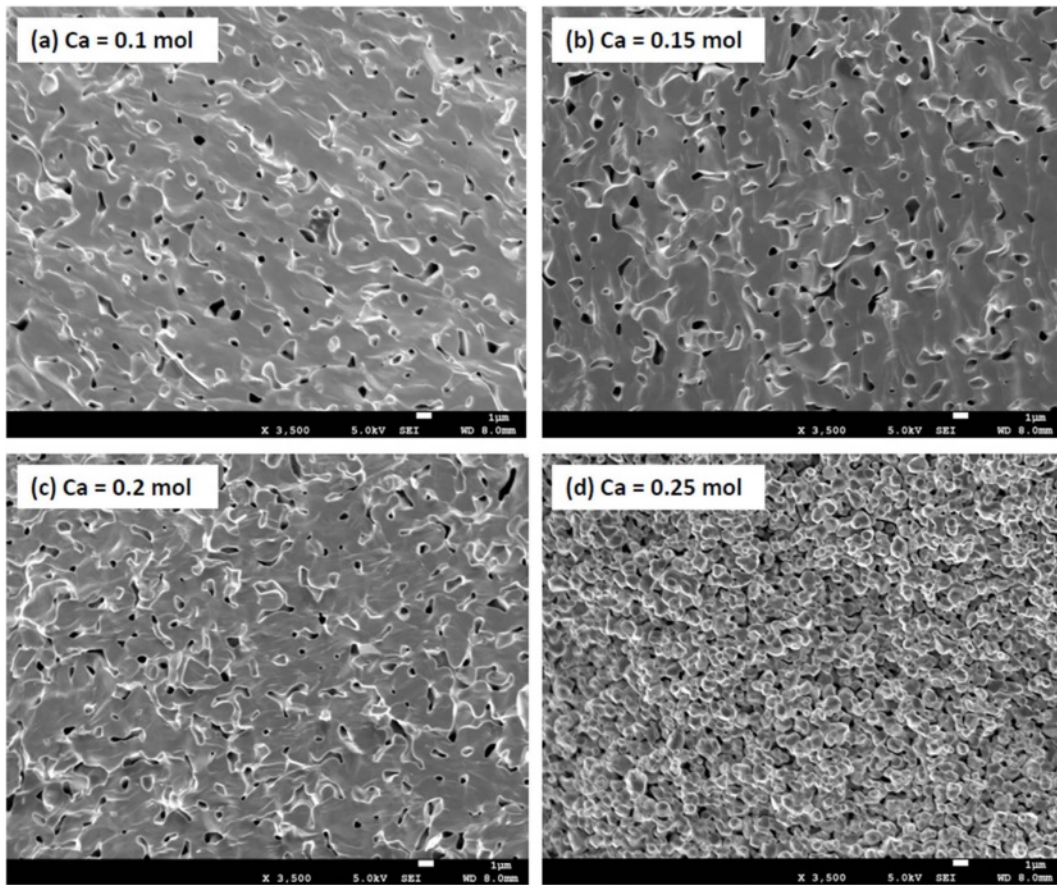


Fig. 3. Microstructure of the LSMO specimens according to the Ca addition amount.

Fig. 4 and Table 1 show the Mn 2p spectra and the orbital binding energies and areas of XPS analysis in Ca-doped LSMO specimens, respectively. The Mn 2p band spectrum is greater than the FWHM of the single valence state [8], which is strong evidence that there is overlap of  $\text{Mn}^{2+}$ ,  $\text{Mn}^{3+}$  and  $\text{Mn}^{4+}$  ions [9]. The  $\text{Mn}^{2+}$ ,  $\text{Mn}^{3+}$  and  $\text{Mn}^{4+}$  ion peaks corresponded with binding energy levels of 640.6-640.7 eV, 641.9-642.1 eV, and 643.2-643.8 eV, respectively. The shape of the Mn 2p signal of the Ca-doped LSMO specimens implies that the majority of the Mn ions are in the  $\text{Mn}^{2+}$  and  $\text{Mn}^{3+}$  states. The Ca composition ratio did not affect the binding energies of the Mn ions and  $\text{Mn}^{3+}/\text{Mn}^{4+}$  ratios.

Fig. 5 shows the resistance-temperature (a) and the resistivity at room temperature (b) of the Ca-doped LSMO specimens. All specimens exhibited typical negative temperature coefficient (NTCR) properties in which resistance decreased linearly as temperature increased. All specimens exhibited good negative temperature coefficient of resistance (NTCR) properties of approximately 0.445-0.421  $\%/\text{C}$ , and the specimen doped with Ca=0.10 mol showed a maximum value of 0.445  $\%/\text{C}$ . For the Ca composition ratio of  $0.1 \leq x \leq 0.2$ , the resistivity was approximately  $4 \times 10^4 \Omega\text{-cm}$ , regardless of the amount of Ca added, but for the specimen with 0.25 mol Ca added, it increased to  $6.07 \times 10^4 \Omega\text{-cm}$ . In

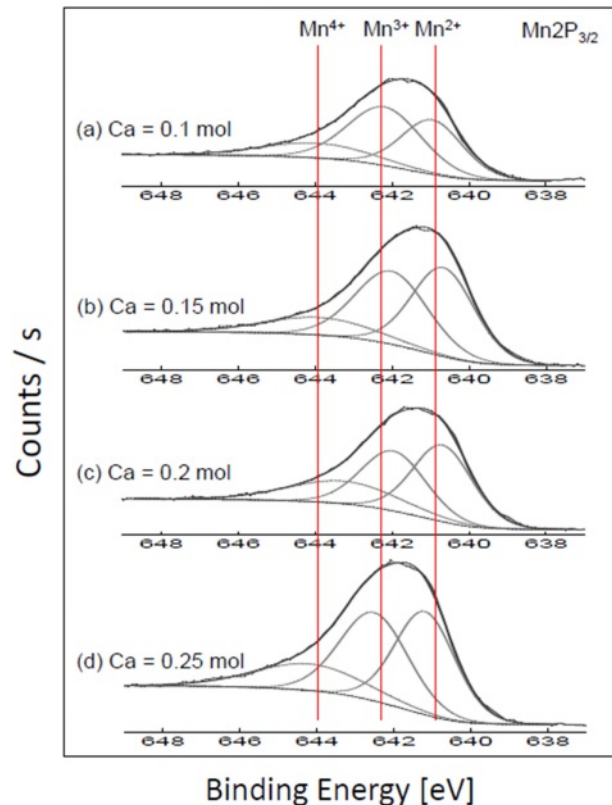
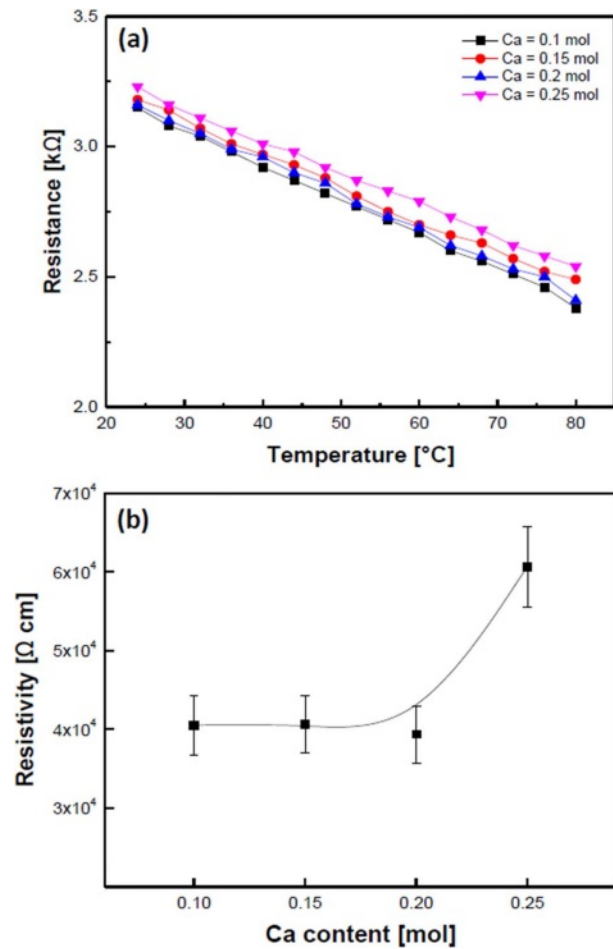


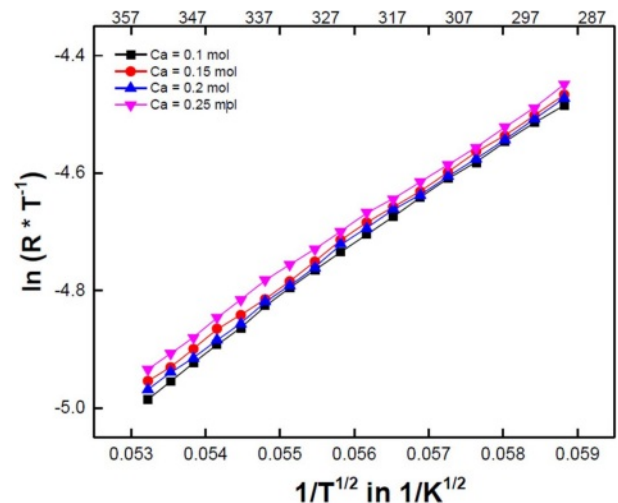
Fig. 4. Mn 2P XPS spectra of Ca-doped LSMO specimens.

**Table 1.** XPS binding energy and peaks area of Ca-doped LSMO specimens.

Ca content	Binding Energy (eV)			Area (%)		
	Mn <sup>2+</sup>	Mn <sup>3+</sup>	Mn <sup>4+</sup>	Mn <sup>2+</sup>	Mn <sup>3+</sup>	Mn <sup>4+</sup>
0.1	640.7	642	643.7	35.88	46.51	17.6
0.15	640.6	642	643.8	43.54	41.28	15.19
0.2	640.6	641.9	643.2	41.8	35.41	22.79
0.25	640.7	642.1	643.7	40.95	39.78	19.27

**Fig. 5.** Resistance-temperature (a) and resistivity at room temperature (b) of the Ca-doped LSMO specimens.

general, the electrical conductivity of manganite crystals depends heavily on their structural properties including pore distribution, secondary phases, and Mn<sup>3+</sup>/Mn<sup>4+</sup> ion ratios. Furthermore, replacing ions with those with a smaller ionic radius in the A-site of ABO<sub>3</sub> perovskite manganite materials reduced the electrical resistance by increasing hopping conduction. This is due to a decrease in the distance between Mn-O ions as a result of the Jahn-Teller lattice distortion of the unit cells [10]. However, in this study, the resistivity increased with an increase in Ca contents because the decrease in grain size and an increase in pore distribution [11], as

**Fig. 6.**  $\ln(R \cdot T^{-1})$  vs.  $1/T^{1/2}$  curves of the Ca-doped LSMO specimens.

shown in Fig. 2.

For ionic bonding manganite crystals, the Jahn-Teller lattice distortion of Mn<sup>3+</sup> cations induces polaron formation through fabrication and impurity additions to specimens. They exhibit high temperature-dependent properties due to Mn<sup>3+</sup>/Mn<sup>4+</sup> small polaron hopping. The temperature-dependent resistance for small polaron hopping conduction is expressed as follows [12]:  $\rho(T) = C_0 \exp(T_0/T)^p$ , where  $C_0$  is a constant, depending on the material properties of the system, and  $T_0$  is a characteristic temperature, which is determined by the slope of the  $\log(R/T)$  vs.  $(1/T)^p$ ; In the case of nearest neighbor hopping (NNH)  $\alpha=p=1$ ; For variable range hopping (VRH)  $\alpha=2p$ ; For Mott VRH hopping  $p=1/4$  [13]; and for Efros-Shklovskii VRH hopping  $p=0.5$  [14]. Fig. 6 shows the  $\ln(R \cdot T^{-1})$  vs.  $1/T^{1/2}$  curves of the Ca-doped LSMO specimens, all of which showed good linearity in the measured temperature range. This means VRH conduction is present, which is thought to be due to the presence of conduction path fluctuations such as grain and grain boundary disorders, random shapes, and porosities as result of variations in the microstructures of bulk specimens [15].

Fig. 7 shows the  $B_{25/65}$  value of the Ca-doped LSMO specimens. The  $B_{25/65}$  value was calculated from the following equation:  $B_{25/65} = (\ln \rho_1 - \ln \rho_2) / (1/T_1 - 1/T_2)$ , where  $\rho_1$  and  $\rho_2$  are the resistances measured at temperature  $T_1$  (25 °C) and  $T_2$  (65 °C), respectively. The B value of the NTC thermistors represents the sensitivity of the change in electrical resistance in relation to the change in temperature. As the Ca composition ratio increased, the B values decreased slightly. The specimen doped with 0.1 mol Ca showed the highest value of 480 K. In general, the smaller the distance between Mn-O ions and the smaller the angle between Mn-O-Mn ions by Jahn-Teller lattice distortion, the higher the conductivity due to the increased probability of hopping to adjacent

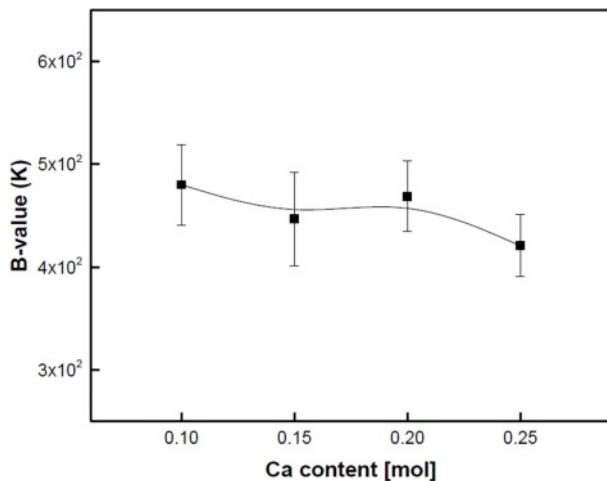


Fig. 7.  $B_{25/65}$  values of the Ca-doped LSMO specimens.

sites. However, in the Ca-doped LSMO specimens, structural properties such as grains, grain boundaries, and pores played a dominant role in the  $B_{25/65}$  value than the conduction mechanism controlled by impurities, as shown in Fig. 5. It is possible to obtain excellent electrical properties if uniform and dense specimens can be produced through changes in manufacturing process conditions.

### Conclusion

The structural and electrical properties of  $\text{La}_{0.7}(\text{Sr}_{0.3-x}\text{Ca}_x)\text{MnO}_3$  ( $0.1 \leq x \leq 0.25$ ) were investigated according to Ca addition amount. The lattice constant decreased as the Ca composition ratio with a small ionic radius increased. When the amounts of Ca added were  $0.1 \leq x \leq 0.2$  and  $x \geq 0.25$ , transgranular fracturing and intergranular fracturing patterns were shown, respectively, which are believed to be due to a decrease in grain size and an increase in pore size. The Ca-doped LSMO ceramics showed VRH conduction, which is believed to be due to the presence of conduction path fluctuations regarding grain and grain boundary disorders, random shapes, and porosities.

### Acknowledgements

This research was supported by Basic Science Research Program through the National Research Foundation of Korea(NRF) funded by the Ministry of Education (2020R1A6A1A03038697) and This work was supported by the National Research Foundation of Korea (NRF) grant funded by the Korea government (MSIT) (2021 R111A3052426).

### References

1. H. Yamada, Y. Ogawa, Y. Ishii, H. Sato, M. Kawasaki, H. Akoh, Y. Tokura, *Science* 305 (2004) 646-648.
2. J.D. Burton and E.Y. Tsymbal, *Phys. Rev. Lett.* 106 (2011) 157203.
3. J. Hemberger, A. Krimmel, T. Kurz, H.A. Krug von Nidda, V.Y. Ivanov, A.A. Mukhin, A.M. Balbashov, and A. Loidl, *Phys. Rev. B* 66 (2002) 094410.
4. M.P. de Jong, I. Bergenti, V.A. Dediu, M. Fahlman, M. Marsi, and C. Taliani, *Phys. Rev. B* 71 (2005) 014434.
5. S. Fritsch, J. Sarrias, M. Brieu, J.J. Couderc, J.L. Baudour, E. Snoeck, and A. Rousset, *Solid State Ionics* 109 (1998) 229-237.
6. M.M. Shokrieh, in "Residual stresses in composite materials" (Woodhead Pub, 2014) p.256-292.
7. S. Uddin, A. Zaman, I. Rassl, S. Akbar, M. Kamran, N. Mehboob, A. Ali, A. Ahmad, M. Nasir, and Z. Iqbal, *J. Ceram. Proc. Res.* 21 (2020) 745-750.
8. H.W. Nesbitt and D. Banerjee, *Am. Miner.* 83 (1998) 305-315.
9. G.M. Bak, C.G. Song, and J.W. Yoon, *J. Ceram. Proc. Res.* 19 (2018) 253-256.
10. J. Wu, Z.M. Huang, Y. Hou, Y.Q. Gao, and J.H. Chu, *J. Chu, Proc. SPIE* 7381 (2009) 738115.
11. A.E. Ghandouri, S. Sayouri, T. Lamcharfi, and L. Hajji, *J. Ceram. Proc. Res.* 19 (2018) 154-170.
12. R. Schmidt, A. Basu, and A.W. Brinkman, *Appl. Phys. Lett.* 86 (2005) 073501.
13. N.F. Mott, in "Conduction in non-crystalline materials" (Oxford, 1993) p.27-32.
14. B.I. Shklovskii and A.L. Efros, in "Electronic Properties of Doped Semiconductors" (Springer, 1984) p.45.
15. R. Schmidt, A. Basu, and A.W. Brinkman, *Phys. Rev. B* 72 (2005) 115101.